

Conference Report

Blind Spots for Direct Detection with Simplified DM Models and the LHC

Arghya Choudhury ^{1,2,*†‡}, Kamila Kowalska ^{3,4,‡}, Leszek Roszkowski ^{1,4,‡}, Enrico Maria Sessolo ^{3,4,‡} and Andrew J. Williams ^{4,‡}

¹ Consortium for Fundamental Physics, Department of Physics and Astronomy, University of Sheffield, Sheffield S3 7RH, United Kingdom

² Consortium for Fundamental Physics, Department of Physics and Astronomy, University of Manchester, Manchester, M13 9PL, United Kingdom

³ Fakultät für Physik, TU Dortmund, Otto-Hahn-Str.4, D-44221 Dortmund, Germany

⁴ National Centre for Nuclear Research, Hoża 69, 00-681 Warsaw, Poland

* Correspondence: a.choudhury@sheffield.ac.uk

† Speaker at "Varying Constants and Fundamental Cosmology" – VARCOSMOFUN'16

‡ Email: a.choudhury@sheffield.ac.uk, kamila.kowalska@tu-dortmund.de, L.Roszkowski@sheffield.ac.uk, enrico.sessolo@ncbj.gov.pl, andrew.williams.2009@live.rhul.ac.uk

Abstract: Using the existing simplified model framework, we build several dark matter models which have suppressed spin-independent scattering cross section. We show that the scattering cross section can vanish due to interference effects with models obtained by simple combinations of simplified models. For weakly interacting massive particle (WIMP) masses $\gtrsim 10$ GeV, collider limits are usually much weaker than the direct detection limits coming from LUX or XENON100. However, for our model combinations, LHC analyses are more competitive for some parts of the parameter space. The regions with direct detection blind spots can be strongly constrained from the complementary use of several Large Hadron Collider (LHC) searches like mono-jet, jets + missing transverse energy, heavy vector resonance searches, etc. We evaluate the strongest limits for combinations of scalar + vector, "squark" + vector, and scalar + "squark" mediator, and present the LHC 14 TeV projections.

Keywords: dark matter; simplified models; direct detection; blind spots; LHC

1. Introduction

Simplified model spectra (SMS) [1–5] have been one of the most popular frameworks for the interpretation of the bounds from mono-photon/mono-jet searches on direct production of dark matter (DM) at the Large Hadron Collider (LHC). In such scenarios, cross section can be parametrized in terms of a few parameters, like the mediator mass or the couplings of the dark matter with the visible sector. Early LHC results were often presented in the effective field theory (EFT) framework, which is a good approximation as long as the mediator masses are well above the collision energy. Various recent studies that analysed the direct detection (DD) and LHC bounds on dark matter have used simplified model scenarios (see, e.g., [2,4]) for this reason and found that in general, for weakly interacting massive particle (WIMP) masses above ~ 5 GeV the limits on spin-independent DM-nucleon cross section (σ_p^{SI}) coming from mono-jet/mono-photon searches are not competitive with the limits from direct detection experiments like LUX [6] or XENON100 [7].

On the other hand, several effects like cascade decays, or cancellations in the couplings, or the interference between different diagrams, which can produce "blind spots" for direct detection searches are not present in the most simple SMS. Thus, the detection issues would be interesting with the models that are halfway between a UV complete model and those SMS. In this work, we combine

three popular SMS in pairs. We only consider the simplified model of DM represented by scalar mediators, colored scalar mediators and vector mediators for which the σ_p^{SI} is significant. In this study we only consider a Dirac fermion dark matter.

In this proceedings, we report on our recent paper [8] in which we dedicated special attention to the direct detection blind spots, which arise from interference between different diagrams in “less simplified” model frameworks (LSMS).

2. The Model Blocks

In this work we present a phenomenological analysis of a three “less simplified” model (LSMS) of DM. These LSMS, to some extent, mimic the properties of more generic UV models.

- **Model 1.** Combining Higgs portal and vector mediators;
- **Model 2.** Combining t -channel scalar mediators (charged under color) and Higgs portal;
- **Model 3.** Combining t -channel scalar mediators (charged under color) and vector mediators.

For these three models, we always consider a Dirac fermion singlet DM. In the next subsections, we briefly recall the characteristics of the three above-mentioned SMS.¹

2.1. Vector Mediator

We consider a leptophobic Z' mediator which has negligible mixing with the SM Z boson. To evade the stringent bounds from LHC di-lepton resonance searches, it has been assumed that Z' also does not couple to the Standard Model leptons.

The relevant interaction terms for DM phenomenology at collider and direct detection experiments are:

$$\mathcal{L} \supset Z'_\mu \bar{\chi} \gamma^\mu (g_\chi^V - g_\chi^A \gamma_5) \chi + \sum_i Z'_\mu \bar{q}_i \gamma^\mu (g_q^V - g_q^A \gamma_5) q_i, \tag{1}$$

where $g_q^V, g_q^A, g_\chi^V, g_\chi^A$ are universal vector quark coupling, universal axial-vector quark coupling, vector and axial-vector couplings to the dark matter respectively. In this study we restrict ourselves to vector boson exchange ($g_{\chi/q}^A = 0$), which contributes σ_p^{SI} . Hence the free parameters become— $m_\chi, m_{Z'}, g_\chi^V$ and g_q^V ; where m_χ is the DM mass and $m_{Z'}$ is the Z' mediator mass. As the product of g_χ^V and g_q^V only matters for σ_p^{SI} , one may reduce the number of free parameters to 3 by assuming $g_\chi^V = g_q^V$.

2.2. Higgs Portal/Scalar Mediator

In this model, it is assumed that the fermion DM singlet (χ) couples to a new singlet real scalar (s). The relevant terms for DM phenomenology are:

$$\mathcal{L} \supset -y_\chi \bar{\chi} \chi s - \mu_s s |\Phi|^2 - \lambda_s s^2 |\Phi|^2, \tag{2}$$

where y_χ is the Yukawa coupling between the singlet and the DM. Mixing between the scalar (s) and the SM Higgs doublet (Φ) is induced by the mass term— μ_s . After electroweak (EW) symmetry breaking, one can diagonalize the mass matrix by a mixing matrix parametrized by a mixing angle θ . Then the relevant interaction terms in the Lagrangian become:

$$\mathcal{L} \supset -y_\chi (h_{SM} \sin \theta + H \cos \theta) \bar{\chi} \chi - \frac{1}{\sqrt{2}} (h_{SM} \cos \theta - H \sin \theta) \sum_f y_f \bar{f} f, \tag{3}$$

¹ Example of Feynman diagrams for Z' , Higgs and squark mediators which provide contributions for monojet signature are given in Figure 1.

where f, \bar{f} are SM fermions and y_f are the SM Yukawa couplings. The DM couples to quarks via the heavy scalar mediator (H), as well as the SM Higgs, h_{SM} . Thus, this type of models are characterized by 4 parameters— $m_\chi, m_H, \sin 2\theta, y_\chi$.

2.3. Scalar t -Channel Mediators

Finally, we consider scalar colored mediators which couple the DM directly to the SM quarks. These scalar mediators are exchanged in the t -channel for DM production at the LHC. Although our model is not based on SUSY, we adopt the notation \tilde{q} which is used to represent the squarks in the Minimal Supersymmetric Standard Model (MSSM). These new scalars are charged under color and flavor. We also assume that masses and couplings for first two generations are universal and the third generation squarks are beyond the reach of LHC.

The relevant terms for DM phenomenology are:

$$\mathcal{L} \supset \sum_{i=1,2} g_{\tilde{q}} \left(\tilde{u}_{i,R}^\dagger \tilde{\chi} P_R u_i + \tilde{u}_{i,L}^\dagger \tilde{\chi} P_L u_i + \tilde{d}_{i,R}^\dagger \tilde{\chi} P_R d_i + \tilde{d}_{i,L}^\dagger \tilde{\chi} P_L d_i \right) + \text{h.c.}, \quad (4)$$

where $\tilde{u}_{i,L(R)}, \tilde{d}_{i,L(R)}, u_i (d_i), P_L (P_R)$ and $g_{\tilde{q}}$ are the i th generation left (right) up-type squarks, the i th generation left (right) down-type squark, the i th generation up (down) quarks, the left (right) chiral projection operators and the coupling strength respectively. The stability of dark matter is assumed to be protected by a discrete symmetry like R-parity. This type of model is characterized by 3 parameters— $m_\chi, m_{\tilde{q}}$ and $g_{\tilde{q}}$, where $m_{\tilde{q}}$ is the universal squark mass and $g_{\tilde{q}}$ is the universal DM-squark coupling.

3. Methodology and Analysis of the Combined Models

Models 1–3 have been implemented using FeynRules [9]. We have calculated σ_p^{SI} using micrOMEGAs v.4.1.8 [10]. For event generation we have used MadGraph5_aMC@NLO [11] and PYTHIA8 [12]. For Model 2–3, we have generated $\chi\bar{\chi}$ + jets, $\chi\tilde{q}$ + jets associated production, and $\tilde{q}\tilde{q}^*$ + jets. To obtain the exclusion limits from jets + missing energy and mono jet searches we have used CheckMATE [13] and our own codes which were previously used in References [14–16]. For 14 TeV projections with jets + missing energy and mono-jet analysis we have followed the prescribed cuts given in References [17,18]. We have also considered the limits on production cross section times branching ratio for $Z' \rightarrow q\bar{q}$ and $Z' \rightarrow t\bar{t}$ from LHC 8 TeV data with 20.3 fb^{-1} [19–21] and the corresponding 14 TeV projections with 300 fb^{-1} [22]. We have calculated the partial width of the 125 GeV Higgs to dark matter particles, $\Gamma_{h_{SM} \rightarrow \chi\bar{\chi}}$, using CalcHEP [23] to compare with the limit from [24]. Considering all these LHC searches, we have compared the upper limits on production cross section times branching ratio or the quantity “upper limits on number of BSM events after all cuts (N_{BSM})” with our models for different values of coupling (e.g., $g_{\chi/q}^V, y_\chi$ etc.) to obtain the new limits.

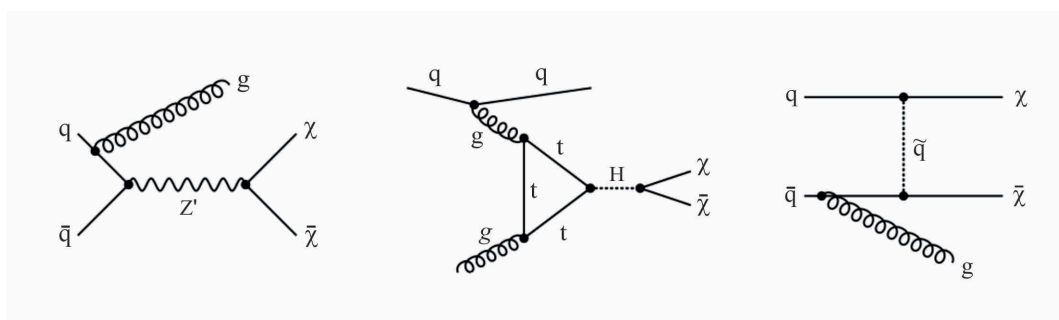


Figure 1. Example of Feynman diagrams for Z' , Higgs and squark mediators which provide contributions for monojet signature.

3.1. Model 1: Combining Z' and Higgs Portal

In the first LSMS (Model 1) we consider a Z' vector boson and an extended scalar sector. Then one can write the relevant terms of Lagrangian as the sum of Equations (1) and (3). With the assumption that $g_\chi^V = g_q^V \equiv g_{\chi/q}^V$ the free parameters (6) become: $m_\chi, m_{Z'}, m_H, \theta, y_\chi, g_{\chi/q}^V$.

We assume mixing as maximal as is allowed by the LHC constraints, perturbativity of the couplings, and EW precision observables: $\theta = 0.2$. The cross section σ_p^{SI} depends mildly on the angle, via $\sin 2\theta$. More detailed analytical formulas for σ_p^{SI} can be found in Reference [8].

In Figure 2a we present the contours of σ_p^{SI} in pb in the $(y_\chi, g_{\chi/q}^V)$ plane for $m_\chi = 10$ GeV, $m_H = 600$ GeV and $m_{Z'} = 1000$ GeV. If $y_\chi > 0$, $m_H \gg m_{h_{\text{SM}}}$, and $g_\chi^V = g_q^V$, destructive interference does not take place (see Equation (3.3)² of Reference [8]). LUX bounds and XENON-1T projected reach are shown by solid red and dashed red lines. Solid (dashed) purple line presents the upper bound from 8 TeV mono-jet searches (14 TeV projected reach). The green solid vertical line provides the upper limit on the y_χ obtained from a ATLAS/CMS combined analysis of $\Gamma_{h_{\text{SM}} \rightarrow \chi\bar{\chi}}$ [24]. The limits from $Z' \rightarrow q\bar{q}$ and $Z' \rightarrow t\bar{t}$ are presented by solid orange line and solid cyan line.

Figure 2 shows that the direct detection limits on coupling ($g_{\chi/q}^V$) from LUX data is more severe than the collider limits in general. Only for $m_\chi \lesssim 62$ GeV, the invisible width of the 125 GeV Higgs boson (green line in Figure 2a,c) is significantly more constraining than the DD bounds. In Figure 2c,d, due to the choice $y_\chi < 0$ (or if it is positive but $g_\chi^V = -g_q^V$), one gets suppressed σ_p^{SI} . This happens due to the destructive interference of the diagrams corresponding to the Higgs portal Z' (see Equation (3.3) of Reference [8]). The blind spot in the plots Figure 2c,d for $m_\chi = 10$ GeV and 100 GeV respectively is a narrow diagonal region, over which the value of σ_p^{SI} visibly drops below the potential reach of tonne-scale detectors. The condition for the blind spot can be written as:

$$y_\chi \approx - \left(\frac{8.22 \times 10^7 \text{ GeV}^2}{m_{Z'}^2} \right) \frac{g_\chi^V g_q^V}{\sin 2\theta \left(1 - \frac{m_{h_{\text{SM}}}^2}{m_H^2} \right)}. \tag{5}$$

Equation (5) shows that the contributions to the amplitude of the diagrams from the Higgs portal and Z' are of comparable size for comparable coupling strengths if $m_{Z'}$ is at least of the order of a TeV or larger. When Condition (5) is satisfied, Model 1 is beyond the reach of direct detection searches but it can be studied by collider means. For this blind spot region, we show the effect of monojet searches, 125 GeV Higgs partial width measurements and Z' resonances searches in the $(m_{Z'}, g_{\chi/q}^V)$ plane in Figure 3 for fixed $m_H = 600$ GeV and two values of DM mass: (a) $m_\chi = 10$ GeV, (b) $m_\chi = 100$ GeV.

The grey regions at the top of Figure 3a are not allowed as y_χ becomes nonperturbative ($y_\chi > 4\pi$). Color coding in Figure 3a is same as in Figure 2. The bounds from the direct Z' resonance searches and the single-jet searches remain almost unchanged over a large range of m_χ . In Figure 3, we observe that the limit from $Z' \rightarrow t\bar{t}$ searches at 8 TeV (solid orange line), $Z' \rightarrow q\bar{q}$ searches [20] at 8 TeV (cyan solid line) and future projection of ATLAS mono-jet searches (dashed purple line) are comparable to each other. For resonant searches, 14 TeV data (dashed orange line) improved significantly on the 8 TeV data for Z' masses above 1500 GeV. In Figure 3b (for fixed $g_{\chi/q}^V = 0.2$), we show that mono-jet search is always weaker than the direct search for a Z' .

² The cancellation can only happen in the nonrelativistic limit. The formula for differential WIMP-nucleus scattering cross section is given in Equation (3.2) of Reference [8] and for the relativistic WIMP-quark scattering see Equation 3.4 of Reference [8].

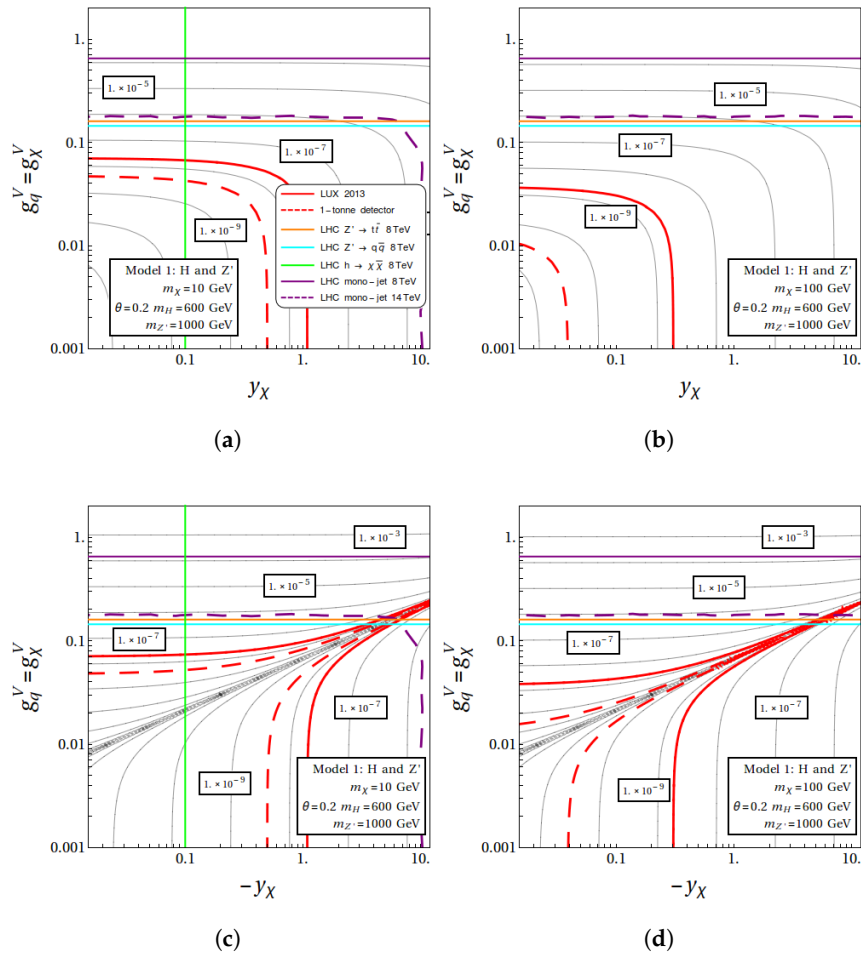


Figure 2. (a) σ_p^{SI} (pb) in the $(y_\chi, g_{\chi/q}^V)$ plane for a Model 1. We set $\theta = 0.2$, $m_\chi = 10$ GeV, $m_{Z'} = 1000$ GeV and $m_H = 600$ GeV. For other details see text; (b) Same as (a) with $m_\chi = 100$ GeV; (c) Same as (a) but the sign of y_χ is negative; (d) Same as (c) but $m_\chi = 100$ GeV.

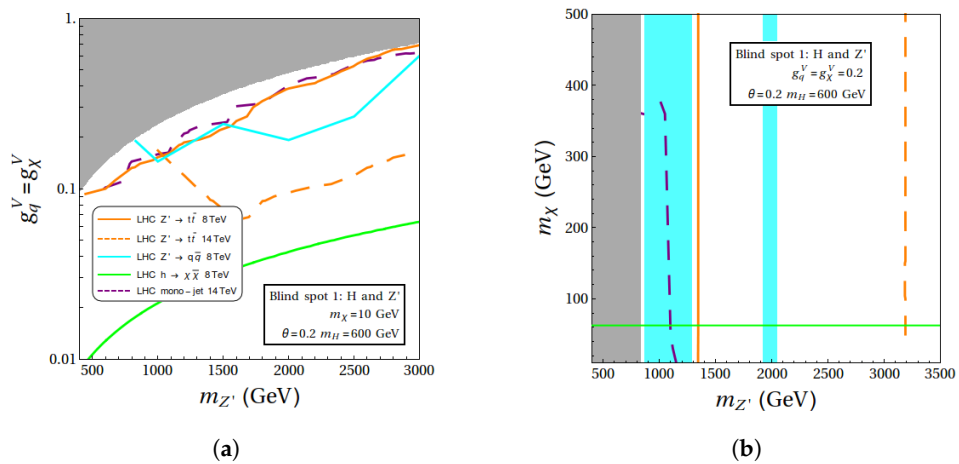


Figure 3. (a) Interplay of collider constraints for the blind spot regions parametrized by Equation (5) in the $(m_{Z'}, g_{\chi/q}^V)$ plane. Here $m_\chi = 10$ GeV, $m_H = 600$ GeV, and $\theta = 0.2$; (b) The bounds projected to the $(m_{Z'}, m_\chi)$ plane for $g_{\chi/q}^V = 0.2$ and $m_H = 600$ GeV. See text for other details.

3.2. Model 2: Combining Higgs Portal and Squarks

Model 2 features some of the properties of SUSY models of DM. In particular the limits are similar to those cases where the neutralino couples to the SM Higgs and additional heavy Higgs bosons. In contrast with MSSM, the DM in our model is a Dirac fermion with free couplings, and the additional scalar is a SM singlet. The relevant terms of Lagrangian for Model 2 is simply the sum of Equations (3) and (4). Hence we have 6 free parameters for Model 2— m_χ , $m_{\tilde{q}}$, m_H , θ , y_χ , $g_{\tilde{q}}$.

We present our results for Model 2 with fixed values of $m_{\tilde{q}} = 1000$ GeV, $\theta = 0.2$, $m_H = 600$ GeV and $m_\chi = 10$ GeV (100 GeV) in Figure 4. Similar to Model 1, cancellations in the amplitude for σ_p^{SI} do not occur for $y_\chi > 0$. Hence, we restrict ourselves for the case $y_\chi < 0$ and one can write the blind spot condition for Model 2 as:

$$y_\chi \approx - \left(\frac{2.05 \times 10^7 \text{ GeV}^2}{m_{\tilde{q}}^2 - m_\chi^2} \right) \frac{g_{\tilde{q}}^2}{\sin 2\theta \left(1 - \frac{m_{h\text{SM}}^2}{m_H^2} \right)}. \tag{6}$$

Figure 4 a,b present the contours of σ_p^{SI} in the $(y_\chi, g_{\tilde{q}})$ plane for $m_\chi = 10$ GeV and $m_\chi = 100$ GeV respectively. The color convention in Figure 4 is exactly same as in Figure 2. Additionally, the upper limit from the ATLAS 8 TeV squarks search in jets + missing E_T [25] is presented by the solid blue line (see also [26] for the CMS bound). Similar to Model 1, the bound on $|y_\chi|$ from the invisible width of the 125 GeV Higgs is much stringent than the DD bounds for $m_\chi < 62.5$ GeV (see green solid line in Figure 4a). This bound from the invisible width does not applicable to Figure 4b and the blind spot regions which are not in reach of underground DD experiments remain essentially unconstrained for $m_\chi \gtrsim 62$ GeV. The dependence of the bounds on $m_{\tilde{q}}$ and m_χ when Equation (6) holds are presented in great details in [8].

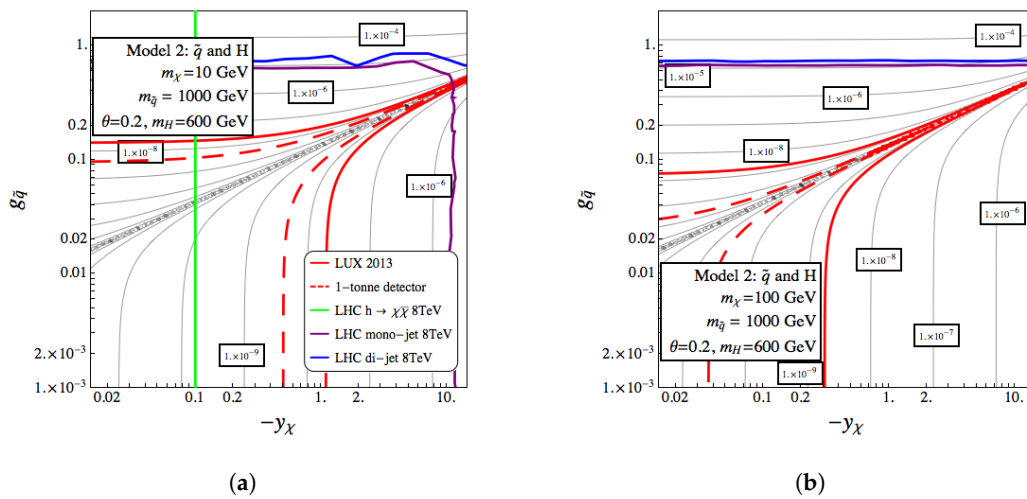


Figure 4. (a) σ_p^{SI} (pb) in the $(y_\chi, g_{\tilde{q}})$ plane for a Model 2. We have fixed $m_\chi = 10$ GeV, $m_{\tilde{q}} = 1000$ GeV, $\theta = 0.2$, and $m_H = 600$ GeV. The full parameter space shown in this figure is within reach of 14 TeV monojet and jets + missing energy searches; (b) Same as (a) but $m_\chi = 100$ GeV.

3.3. Model 3: Combining Z' and Squarks

We have designed Model 3 to mimic a UV completion characterized by an additional $U(1)_X$ symmetry that remains unbroken down to collider energies (see, e.g., [27]). Among the several possibilities, one way of building a gauge invariant LSMS with the squarks and Z' mediated simplified models is the following, which allows the squarks to have the same coupling to the Z' as the quarks, and could be seen as an approximation of a full UV theory involving an extended gauge symmetry and

a supersymmetric sector (for details see Section 3.3 of Reference [8]). Despite being apparently rather involved, the phenomenology of Model 3 is represented by 6 free parameters— $m_\chi, m_{\tilde{q}}, m_{Z'}, g_\chi^V, g_q^V, g_{\tilde{q}}$. With the additional assumption $g_\chi^V = \pm g_q^V \equiv g_{\chi/q}^V$, this number is further reduced to 5.

We show the σ_p^{SI} contours in Figure 5a for Model 3 in the $(g_{\chi/q}^V, g_{\tilde{q}})$ plane for fixed $m_{\tilde{q}} = 1000$ GeV and $m_{Z'} = 1000$ GeV. Color conventions are same as Figure 2 or Figure 4. The case with $m_\chi = 100$ GeV is shown in Figure 5b. It may be noted that the LHC limits barely move by changing the DM mass, but direct detection limits reach their close-to-maximal strength when $m_\chi = 100$ GeV. The jets + missing energy and mono-jet searches put comparable constraints on the couplings (blue and purple line). The interplay of LHC limits on the mediators' mass for blind spot regions are discussed in details in Section 3.3 of Reference [8]. A complementary use of different detection strategies is needed to constrain a large part of the parameter space which is invisible in direct detection experiments.

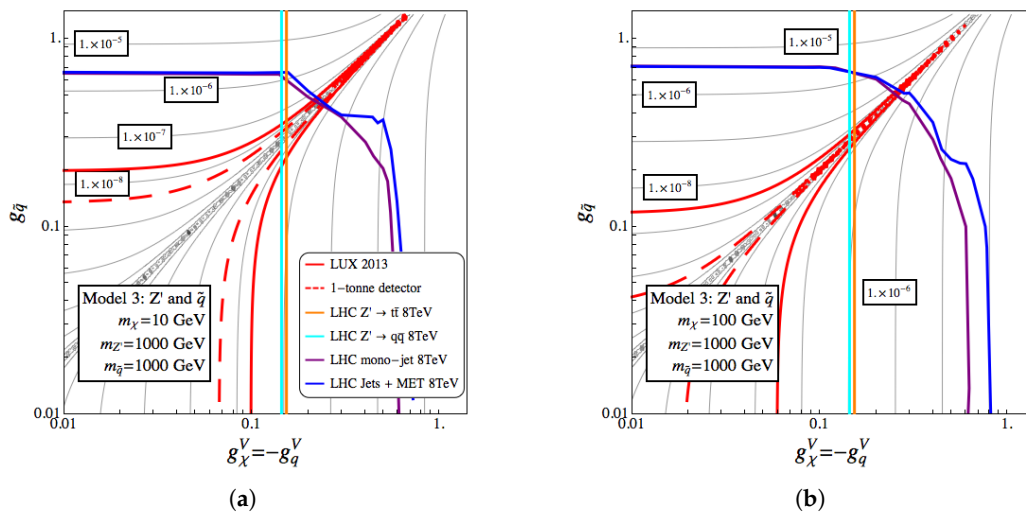


Figure 5. (a) σ_p^{SI} (pb) in the $(g_\chi^V = -g_q^V, g_{\tilde{q}})$ plane for a combined Model 3 (Z' + squark mediator simplified model). The masses are fixed at $m_\chi = 10$ GeV, $m_{Z'} = 1000$ GeV, and $m_{\tilde{q}} = 1000$ GeV; (b) Same as (a) but $m_\chi = 100$ GeV.

4. Summary and Conclusions

In this work we have presented three dark matter models (LSMS) which are simple extensions of simplified DM models and mimic some properties of more realistic models without introducing an excessively large number of parameters. We mainly focussed to the scenarios where the interference between different diagrams produces blind spot for direct detection experiments. These blind spot regions are then further tested with current LHC limits and also with future LHC projections.

In general for $m_\chi \geq 10$ GeV, the DD bounds on σ_p^{SI} excludes the coupling constants of WIMP by at least one order of magnitude more strongly than any of the LHC searches considered here. The exceptions are: (i) In models with a Higgs portal (Model 1 and Model 2), for $m_\chi \lesssim 1/2 m_{h_{\text{SM}}}$ the parameter space is also strongly constrained by the invisible width of the 125 GeV Higgs boson; (ii) In the parameter space corresponding to suppressed σ_p^{SI} due to interference effect, i.e., blind spot regions, LHC searches can effectively place strong bounds, especially at the end of Run 2.

We have found the following characteristics for the blind spot regions of Models 1–3:

- The Model 1 (combination of Higgs portal and Z') is at present not constrained at all by mono-jet searches for the assumption $g_\chi^V = g_q^V$. Moreover, under this assumption, the future searches of heavy Z' resonances at the LHC will be most effective to probe the blind spot regions.
- In Model 2 and Model 3 (involving squark-like mediators), the current limits on the coupling $g_{\tilde{q}}$ from jets + missing energy and mono-jet searches are comparable. However, according to LHC

future projections [17,18], the jets + missing energy searches at the 14 TeV LHC will outperform the expectations for mono-jet searches in the parameter space with blind spots.

In general we find that, to constrain the DM models at the colliders, it is crucial to use the complementarity of different search strategies. A lot of well motivated DM models, which are not necessarily constrained by DD bounds, demand careful attention at LHC or future colliders. In this work, we have investigated such scenarios in terms of a less-simplified model framework which can be explored at the LHC.

Acknowledgments: A.C. and L.R. are supported by the Lancaster-Manchester-Sheffield Consortium for Fundamental Physics under STFC Grant No. ST/L000520/1. K.K. is supported in part by the DFG Research Unit FOR 1873 “Quark Flavour Physics and Effective Field Theories”. L.R. and E.M.S. are supported in part by the National Science Council (NCN) research grant No. 2015-18-A-ST2-00748. The work of E.M.S. is supported in part by the Alexander von Humboldt Foundation. The use of the CIS computer cluster at the National Centre for Nuclear Research in Warsaw is gratefully acknowledged.

References

1. Goodman, J.; Shepherd, W. LHC Bounds on UV-Complete Models of Dark Matter **2011**. [[arXiv:hep-ph/1111.2359](#)].
2. Abdallah, J.; others. Simplified Models for Dark Matter and Missing Energy Searches at the LHC **2014**. [[arXiv:hep-ph/1409.2893](#)].
3. Malik, S.A.; others. Interplay and Characterization of Dark Matter Searches at Colliders and in Direct Detection Experiments. *Phys. Dark Univ.* **2015**, *9-10*, 51–58, [[arXiv:hep-ex/1409.4075](#)].
4. Abdallah, J.; others. Simplified Models for Dark Matter Searches at the LHC. *Phys. Dark Univ.* **2015**, *9-10*, 8–23, [[arXiv:hep-ph/1506.03116](#)].
5. Abercrombie, D.; others. Dark Matter Benchmark Models for Early LHC Run-2 Searches: Report of the ATLAS/CMS Dark Matter Forum **2015**. [[arXiv:hep-ex/1507.00966](#)].
6. Akerib, D.S.; others. First results from the LUX dark matter experiment at the Sanford Underground Research Facility. *Phys. Rev. Lett.* **2014**, *112*, 091303, [[arXiv:astro-ph.CO/1310.8214](#)].
7. Aprile, E.; others. Dark Matter Results from 225 Live Days of XENON100 Data. *Phys. Rev. Lett.* **2012**, *109*, 181301, [[arXiv:astro-ph.CO/1207.5988](#)].
8. Choudhury, A.; Kowalska, K.; Roszkowski, L.; Sessolo, E.M.; Williams, A.J. Less-simplified models of dark matter for direct detection and the LHC. *JHEP* **2016**, *04*, 182, [[arXiv:hep-ph/1509.05771](#)].
9. Alloul, A.; Christensen, N.D.; Degrande, C.; Duhr, C.; Fuks, B. FeynRules 2.0 - A complete toolbox for tree-level phenomenology. *Comput. Phys. Commun.* **2014**, *185*, 2250–2300, [[arXiv:hep-ph/1310.1921](#)].
10. Belanger, G.; Boudjema, F.; Pukhov, A.; Semenov, A. micrOMEGAs 3: A program for calculating dark matter observables. *Comput. Phys. Commun.* **2014**, *185*, 960–985, [[arXiv:hep-ph/1305.0237](#)].
11. Alwall, J.; Frederix, R.; Frixione, S.; Hirschi, V.; Maltoni, F.; others. The automated computation of tree-level and next-to-leading order differential cross sections, and their matching to parton shower simulations. *JHEP* **2014**, *1407*, 079, [[arXiv:hep-ph/1405.0301](#)].
12. Sjostrand, T.; Mrenna, S.; Skands, P.Z. A Brief Introduction to PYTHIA 8.1. *Comput. Phys. Commun.* **2008**, *178*, 852–867, [[arXiv:hep-ph/0710.3820](#)].
13. Drees, M.; Dreiner, H.; Schmeier, D.; Tattersall, J.; Kim, J.S. CheckMATE: Confronting your Favourite New Physics Model with LHC Data. *Comput. Phys. Commun.* **2014**, *187*, 227–265, [[arXiv:hep-ph/1312.2591](#)].
14. Kowalska, K.; Roszkowski, L.; Sessolo, E.M.; Williams, A.J. GUT-inspired SUSY and the muon g-2 anomaly: prospects for LHC 14 TeV. *JHEP* **2015**, *06*, 020, [[arXiv:hep-ph/1503.08219](#)].
15. Chakraborti, M.; Chattopadhyay, U.; Choudhury, A.; Datta, A.; Poddar, S. The Electroweak Sector of the pMSSM in the Light of LHC - 8 TeV and Other Data. *JHEP* **2014**, *07*, 019, [[arXiv:hep-ph/1404.4841](#)].
16. Chakraborti, M.; Chattopadhyay, U.; Choudhury, A.; Datta, A.; Poddar, S. Reduced LHC constraints for higgsino-like heavier electroweakinos. *JHEP* **2015**, *11*, 050, [[arXiv:hep-ph/1507.01395](#)].
17. Sensitivity to WIMP Dark Matter in the Final States Containing Jets and Missing Transverse Momentum with the ATLAS Detector at 14 TeV LHC. Technical Report ATL-PHYS-PUB-2014-007, CERN, Geneva, 2014.

18. Search for Supersymmetry at the high luminosity LHC with the ATLAS experiment. Technical Report ATL-PHYS-PUB-2014-010, CERN, Geneva, 2014.
19. Aad, G.; others. A search for $t\bar{t}$ resonances using lepton-plus-jets events in proton-proton collisions at $\sqrt{s} = 8$ TeV with the ATLAS detector. *JHEP* **2015**, *08*, 148, [arXiv:hep-ex/1505.07018].
20. Aad, G.; others. Search for new phenomena in the dijet mass distribution using $p - p$ collision data at $\sqrt{s} = 8$ TeV with the ATLAS detector. *Phys. Rev.* **2015**, *D91*, 052007, [arXiv:hep-ex/1407.1376].
21. Aad, G.; others. Search for new phenomena in dijet mass and angular distributions from pp collisions at $\sqrt{s} = 13$ TeV with the ATLAS detector. *Phys. Lett.* **2016**, *B754*, 302–322, [arXiv:hep-ex/1512.01530].
22. Studies of Sensitivity to New Dilepton and Ditop Resonances with an Upgraded ATLAS Detector at a High-Luminosity LHC. Technical Report ATL-PHYS-PUB-2013-003, CERN, Geneva, 2013.
23. Belyaev, A.; Christensen, N.D.; Pukhov, A. CalcHEP 3.4 for collider physics within and beyond the Standard Model. *Comput. Phys. Commun.* **2013**, *184*, 1729–1769, [arXiv:hep-ph/1207.6082].
24. Measurements of the Higgs boson production and decay rates and constraints on its couplings from a combined ATLAS and CMS analysis of the LHC pp collision data at $\sqrt{s} = 7$ and 8 TeV. Technical Report ATLAS-CONF-2015-044, CERN, Geneva, 2015.
25. Aad, G.; others. Search for squarks and gluinos with the ATLAS detector in final states with jets and missing transverse momentum using $\sqrt{s} = 8$ TeV proton-proton collision data. *JHEP* **2014**, *09*, 176, [arXiv:hep-ex/1405.7875].
26. Khachatryan, V.; others. Searches for supersymmetry using the M_{T2} variable in hadronic events produced in pp collisions at 8 TeV. *JHEP* **2015**, *05*, 078, [arXiv:hep-ex/1502.04358].
27. Athanasopoulos, P.; Faraggi, A.E.; Mehta, V.M. Light Z' in heterotic string standardlike models. *Phys. Rev.* **2014**, *D89*, 105023, [arXiv:hep-th/1401.7153].



© 2017 by the authors. Licensee MDPI, Basel, Switzerland. This article is an open access article distributed under the terms and conditions of the Creative Commons Attribution (CC BY) license (<http://creativecommons.org/licenses/by/4.0/>).